Journal of Materials Chemistry A

Accepted Manuscript

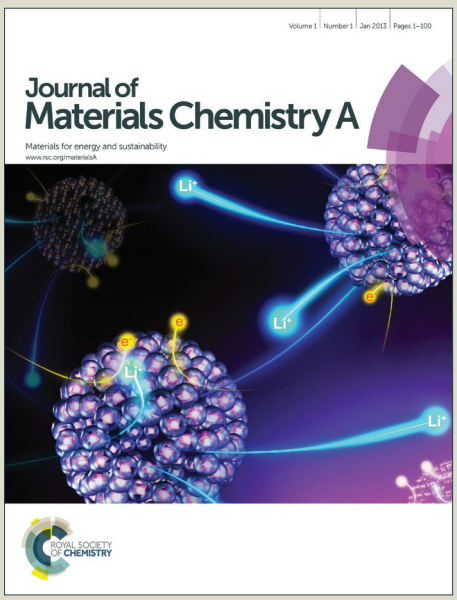

ROYAL SOCIETY OF CHEMISTRY

www.rsc.org/materialsA

Journal Name

RSCPublishing

ARTICLE

One-Pot and General Synthesis of Well Crystalline Mesoporous Metal Oxides Nanoparticles by Protective Etching: Potential Materials for Catalytic Applications

Cite this: DOI: 10.1039/xoxxoooooox

Received ooth January 2012,
Accepted ooth January 2012

DOI: 10.1039/xoxxoooooox

www.rsc.org/

Nating Yang,[a] Fei Pang [b] and Jianping Ge [a, b, *]

A one-pot protective etching process was developed to prepare several mesoporous metal oxides, including CeO_2, Cu_2O and ZnO. Polycrystalline precursor particles, protective agent with proper combination to precursor and etchant with matched etching capability are three preconditions to construct the protective etching system. Compared to previous approaches, the current method has several advantages simultaneously, which includes compatibility for different metal oxides, one-pot reaction without multi-step procedures, fast synthesis (3 hour) from common metal salts to porous products, large surface area (up to 200 m^2/g) and well crystalline porous framework. The mesoporous CeO_2 loaded with Pt catalyst show better activity, higher selectivity, longer life and good thermo stability in CO oxidation compared to CeO_2-Pt catalyst, which reveals its potential in large scale production of abundant materials for catalytic applications.

1. Introduction

Mesoporous structure has attracted great interests due to the high surface area, tunable pore size, and selective diffusion within the pores. In the past decade, people have synthesized mesoporous materials with various chemical compositions, such as silica, carbon, metal oxides, phosphates, sulphides, nitrides and polymers, etc.[1, 2] Among these materials, the porous metal oxides present great potentials for applications[3] in catalysis,[4-6] energy storage/ conversion[7-12] and electrochemical sensors.[13, 14] For example, as heterogeneous catalyst, mesoporous Cu/CeO_2 obtained from nanocasting of silica template has high surface area (200 m^2/g) and large pore size (16 nm), which can drive a complete conversion and 100 % of selectivity in the preferential oxidation of carbon monoxide at 40 °C.[4] As an anode material for lithium-ion batteries, mesoporous NiO with surface area of 96 m^2/g exhibits lower activation energy and higher specific capacity than the bulk NiO.[10] As a sensing material, mesoporous In_2O_3 with surface area of 90 m^2/g has good thermal stability up to 650 °C, which renders it superior sensitivity and selectivity in response to methane gas.[13]

Traditional methods for the synthesis of mesoporous metal oxides include nanocasting (hard template),[2, 15-17] soft template assembly,[18-22] topological transformation,[23-25] MOF conversion,[26-29] solvothermal reaction[30-33] and artificial stacking of nanosize building blocks.[34] For instance, mesoporous metal oxides (Cr_2O_3, Mn_xO_y, Fe_2O_3, Co_3O_4, NiO & In_2O_3) with surfaces areas of 50-140 m^2/g can be prepared by introduction of precursor into the mesoporous silica template, calcination in air to generate metal oxides, and removal of template in NaOH solution.[15] In addition to nanocasting, mesoporous ZnO with surface area of 456 m^2/g can be prepared by using zinc chloride and hexadecyl-2-pyridinyl-methylamine as precursor and soft template respectively. Porous ZnO were obtained after 50 hours of reaction and aging at 0 °C, followed by the template removal in ethanol-HCl solution.[21] In some cases, mesoporous metal oxide can be synthesized by topotactic transformation of single crystal precursors. When flower-like cobalt carbonate hydroxide is calcinated at 300 °C in air, it turns to quasi-single-crystalline Co_3O_4 nanowires with surface area of 20-30 m^2/g.[24] In a similar strategy, hierarchically nanoporous MgO and CeO_2 can be prepared by thermolysis of aliphatic ligand-based MOF under inert atmosphere.[26] Furthermore, solvothermal method was developed to prepare mesoporous CeO_2 with high surface area (216 m^2/g), which is produced by heating the mixture of cerium nitrate, water, glycol and acetic acid at 180 °C for 200 min.[30] Finally, mesoporous metal oxides (Fe_3O_4, ZrO_2) can also be prepared by the stacking of premade monodisperse nanocrystals, which is realized by construction of micro-emulsion oil droplets containing nanocrystals and evaporation of solvent to facilitate the self-assembly.[34] Although these methods have greatly enriched the synthetic approaches to mesoporous metal oxides, they all have their own limitation in the aspects of synthesis easiness and efficiency or products porosity and crystallinity. Therefore, it is still a challenge to develop a general method, which can produce various metal oxides with high surface area and good crystallinity through straightforward and time saving procedures.

Recently, Yin et al. have reported the synthesis of mesoporous silica using a protective etching strategy.[35, 36] In their work, dense silica coated with PVP molecules are etched by NaOH to generate porous silica or even hollow silica vesicle due to different etching speed between the interior or surface part of the particle. This method is convenient to obtain silica materials with abundant disordered mesopores. However, it is limited to the case of silica

only and it is unsuitable for the synthesis of mesoporous transition metal oxides because most of them are stable in basic solutions. Inspired by the success of protective etching of silica, we are wondering whether this strategy can be extended to the synthesis of mesoporous metal oxides under a framework of acid etching reaction.

In this work, mesoporous metal oxides including CeO_2, Cu_2O and ZnO are prepared by controlled etching of PVP protected oxide precursors with low amount of inorganic acid. Acid etching has already been used to prepare porous or hollow nanostructures, where a metal/oxide core/shell precursor is generally required for the selective removal of metal component by reacting with acid, leaving behind a porous oxide framework.[37, 38] However, the current method needs no specific composite precursor and it can be applied to prepare several mesoporous metal oxides via straightforward reaction route. Here, the polyol synthesized particles are chosen as precursors for protective etching since they are composed of secondary nanocrystals and coated with polymeric surfactant.[39] As to be discussed later, the cluster-like structures of polyol particles and the surface protection by surfactant are the keys to forming the mesoporous materials. Therefore, mesoporous metal oxides can be conveniently prepared through a one-pot reaction, which seamlessly combine the polyol synthesis with the protective etching.

Compared to all previous approaches, the current method has several advantages simultaneously, which includes compatibility for different metal oxides, one-pot reaction without multi-step procedures, fast synthesis (3 hour) from common metal salts to mesoporous products, large surface area (up to 200 m^2/g) and well crystalline porous framework. The large surface area and good crystallinity of the as-made mesoporous metal oxides render them superior properties in catalysis. As a demonstration, Pt nanocatalysts loaded on unetched and etched CeO_2 particles are compared in the catalytic oxidation of CO, and the mesoporous support exhibit better performance in the aspects of activity, selectivity, life time and thermo stability, which reveals the potential of protective etching in catalyst production.

2. Experimental Section

2.1 Materials

Cerium (III) nitrate hexahydrate ($Ce(NO_3)_3 \cdot 6H_2O$, 99.5%), cerium (III) chloride heptahydrate ($CeCl_3 \cdot 7H_2O$, 99.9%) and zinc acetate dehydrate ($Zn(Ac)_2 \cdot 2H_2O$, 99.99%) was obtained from Aladdin Co. Ltd. Polyvinyl pyrrolidone (PVP, Mw=29,000), chloroplatinic acid hexahydrate ($H_2PtCl_6 \cdot 6H_2O$, Pt ≥ 37.5%), diethylene glycol (DEG, 99%) and L-asorbic acid (99%) were purchased from Sigma Aldrich. Ethylene glycol (EG, 99%) were purchased from J&K Co. Ltd. Hydrochloric acid (HCl, 37%), sulfuric acid (H_2SO_4, 95~98%), sodium hydroxide (NaOH, AR), ethanol (99.7%), polyvinyl pyrrolidone (PVP, K30) and copper (II) acetate monohydrate ($Cu(Ac)_2 \cdot H_2O$, AR) were obtained from the Sinopharm Chemical Reagent Co. Ltd. All chemicals were used without further purification.

2.2 Synthesis of CeO_2, Cu_2O and ZnO nanoparticles

CeO_2 nanoparticles with average diameter of 110 nm were prepared through a high temperature polyol process modified from the literature method.[39] Typically, PVP (Mw=29000, 31.5 mmol) and $Ce(NO_3)_3 \cdot 6H_2O$ (5 mmol) were dissolved in EG (20 mL) at 70 °C, which was gradually heated to 155 °C under N_2 protection. The transparent yellowish solution gradually turned to yellow slurry in 15 min after the reaction temperature was reached, and the mixture was aged for another 45 min to produce well crystallized CeO_2 nanoparticles. After cooling the reaction solution down to room temperature, the suspension of CeO_2 nanoparticles was directly stocked in glass vessels for the following etching process. In order to prepare CeO_2 based catalysts, the nanoparticles were diluted with ethanol, separated from the solution by centrifugation, washed with ethanol and water for 3 times and dried in vacuum to generate yellow powders.

For the preparation of 190-nm Cu_2O nanoparticles, a modified polyol method from literature[40, 41] was used. PVP (K30, 40 mmol) dissolved in DEG (70 mL) was first heated to 180 °C under N_2 protection. Then, $Cu(Ac)_2 \cdot H_2O$ (4 mmol) dissolved in DEG (8 mL) was injected into the above hot solution to initiate the generation of Cu_2O. The transparent bluish green solution rapidly turned to orange slurry in 5 min, and the mixture was further stirred at 180 °C for another 2 h to accomplish the reaction. The following separation and purification was similar to the procedures applied in case of CeO_2 synthesis.

In order to prepare ZnO-1 nanoparticles with average diameter of 160 nm and crystal grain size of 6.7 nm. L-Asorbic acid (0.284 mmol) and PVP (K30, 12.4 mmol) were first dissolved in DEG (50 mL) at 180 °C under N_2 protection. Then, $Zn(Ac)_2 \cdot 2H_2O$ (5 mmol) dissolved in DEG (5 mL) was injected into the above hot solution. The transparent brown solution gradually turned to yellowish white in 15 min, and the mixture was further stirred at 180 °C for another 2 h. The following separation and purification was similar to the procedures applied in case of CeO_2 synthesis. The synthesis was extended from the above strategies and not from the literatures.

In order to prepare ZnO-2 nanoparticles[42] with average diameter of 250 nm and crystal grain size of 13.4 nm, $Zn(Ac)_2 \cdot 2H_2O$ (15 mmol) and PVP (K30, 48 mmol) was dissolved in DEG (160 mL) at 60 °C and the solution was heated to 160 °C under N_2 protection. The colorless and transparent solution gradually turned to milky white in 30 min, and the mixture was aged at 160 °C for another 2.5 h. The following separation and purification was similar to the procedures applied in case of CeO_2 synthesis.

2.3 Synthesis of mCeO_2, mCu_2O and mZnO nanoparticles

For the synthesis of mCeO_2, the reaction solution in section 2.2 containing EG (12.5 mL), PVP (16 mmol) and CeO_2 particle (2.5 mmol) were loaded to a sealed flask, heated to 120 °C and maintained at that temperature for 10 min. Then, an aqueous solution of HCl (0.34 mL, 12 M) was quickly injected to the dispersion to initiate the etching. Along with the etching process, the yellow slurry gradually turns to pale yellow and transparent dispersion within the following 2 hours. The mCeO_2 particles with different porosities can be obtained by ceasing the etching at specific reaction time, cooling the solution down to room temperature and washing the particles with excessive ethanol and water.

For the synthesis of mCu_2O, the reaction solution in section 2.2 containing DEG (50 mL), PVP (25 mmol) and Cu_2O particles (1.25 mmol) was heated to 90 °C and maintained at that temperature for 10 min. Then, an appropriate amount of aqueous solution of H_2SO_4 (0.025 - 0.125 mL, 9.2 M) was quickly injected to the dispersion to initiate the etching, and the solution was stirred at 90 °C for another 30 min to produce mesoporous Cu_2O particles. The products' porosity can be tuned by the concentration of H_2SO_4 in etching.

For the preparation of mZnO-1, the reaction solution in section 2.2 containing DEG (20 mL), PVP (4 mmol) and ZnO-1 particles (1.6 mmol) was heated to 120 °C and maintained at that temperature for 10 min. Then, an aqueous solution of HCl (0.05 - 0.15 mL, 12 M) was quickly injected to the dispersion to initiate the etching, and the mesoporous ZnO particles were obtained after 20-min reaction.

For the preparation of mZnO-2, the reaction solution in section 2.2 containing DEG (40 mL), PVP (12 mmol) and ZnO-2 particles (3.75 mmol) was heated to 120 °C and maintained at that temperature for 10 min. Then, an aqueous solution of HCl (0.35 - 0.375 mL, 12 M)

was quickly injected to the dispersion to initiate the etching, and the mesoporous ZnO particles were obtained after 5-min reaction. Similarly, the porosity can be tuned by the concentration of HCl in etching.

2.4 Loading Pt catalyst to CeO_2 and $mCeO_2$ nanoparticles

The Pt-CeO_2 and Pt-$mCeO_2$ catalysts were prepared using a modified impregnation method. For the preparation of catalysts loaded with 3wt% of Pt, $H_2PtCl_6{\cdot}6H_2O$ (0.063 mmol) was dissolved in ethanol to form a transparent and yellow solution, which was added dropwise to the dried CeO_2 or $mCeO_2$ powders (2.33 mmol). The wet powders were dried in vacuum for 3 hours and in oven at 60 °C for another 3 hours to guarantee the removal of ethanol. The samples were calcinated in dry air for 4 hours by a tubular furnace at 500 °C (or 700 °C) to decompose H_2PtCl_6 into oxides, which were further reduced in H_2/Ar flow (5%) for 1 hour at 300 °C to produce the final catalysts.

2.5 CO oxidation catalysed by Pt-CeO_2 and Pt-$mCeO_2$

For the evaluation of CeO_2 based nanocatalysts, 50 mg of catalysts (40-60 mesh) were first loaded in a U-shaped quartz microreactor with internal diameter of 3.8 mm and pretreated in H_2 flow (50 mL·min^{-1}) at 120 °C for 1 hour. After introducing the feed gas (2.0 % CO and 2.0 % O_2 diluted in N_2) with a flow rate of 50 mL·min^{-1} into the reactor, the reaction temperature was raised from 30 to 100 °C following a programmed heating procedure. With a step of 10 °C, the system was maintained at the test temperature for 5 min before the gaseous products were sampled and analyzed. It should be noted that a mixture of CO, O_2 N_2 and H_2 with volume ratio of 1:1:48:50 was used as feed gas in the preferential oxidation of CO. For the test of catalyst stability, the catalyst amount was reduced to about 3 mg, the feed gas flow rate was increased to 200 mL·min^{-1} and the catalysis was performed from 120 to 240 °C. Detailed experimental parameters including the catalyst compositions, the flow rate of feed gases and the reaction temperature for different catalytic reactions were summarized in Table 5. The gaseous products sampled by the six-way valve were analyzed by a GC equipped with TDX-01 column and TCD detector. Conversions, selectivity and turnover frequency of CO oxidation were calculated according to the following equations: $C = [n(CO_{in}) - n(CO_{out})] / n(CO_{in})$; $S = [n(CO_{in}) - n(CO_{out})] / [n(CO_{in}) - n(CO_{out}) + n(H_{2in}) - n(H_{2out})]$;[43] $TOF = [n(CO_{in}) - n(CO_{out})] / (n_{(Pt)} * t)$.

2.6 Characterizations

The morphological evolution of $mCeO_2$ particles during the etching process was characterized by a JEOL JEM-2100 transmission electron microscope (TEM) operated at 200 kV. Nitrogen adsorption-desorption isotherms, BET surface areas and BJH pore diameters were measured at 77 K with a Belsorp-Max analyzer. All the samples were degassed in N_2 flow at 150 °C (120 °C for the ceria samlpes) for 2 h before the test. X-ray diffraction (XRD) patterns were recorded on a Rigaku Ultima VI X-ray diffractometer operated at 35 kV and 40 mA with Cu-Kα radiation as beam source, scanning from 10° to 80° with a speed of 60 degree per minute. The loading amount of Pt catalyst on CeO_2 support was measured by Thermo IRIS Intrepid II XSP Inductive Couple Plasma Atomic Emission Spectrometer (ICP-AES). The elementary distribution of the Pt-$mCeO_2$ nanocatalysts was analyzed by Hitachi S4800 scanning electron microscope (SEM) equipped with EDS module. The FT-IR spectra of the samples were measured by Nicolet FT-IR 560 spectrometer.

3. Results and Discussion

Mesoporous metal oxide nanoparticles are prepared through a protective etching process, which uses polyol synthesized particles as precursor, PVP as protective agent and low-concentration acid as etchant. (Figure 1) As a typical example, solid CeO_2 particles are first synthesized by hydrolysing metal salts in glycols at high temperature. Uniform particles are produced by the wrapping of PVP molecules, which naturally function as protective agent in the following etching process. Without additional separation or purification, droplets of HCl aqueous solution are directly added to the above solution at 120 °C to initiate the etching. Along with etching, the solid particles gradually transformed to mesoporous and then hollow particles. (Figure 2) The final products with different porosities can be obtained by ceasing the reaction at specific time, cooling down the solution and separating the particles by centrifugation. (Table 1)

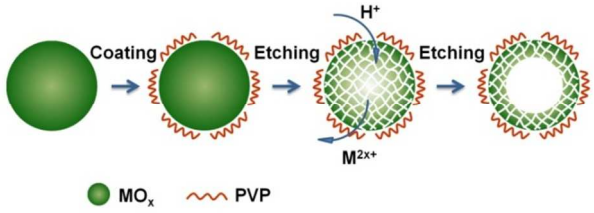

Figure 1. Schematic illustration to the synthesis of mesoporous metal oxide particles via protective etching process.

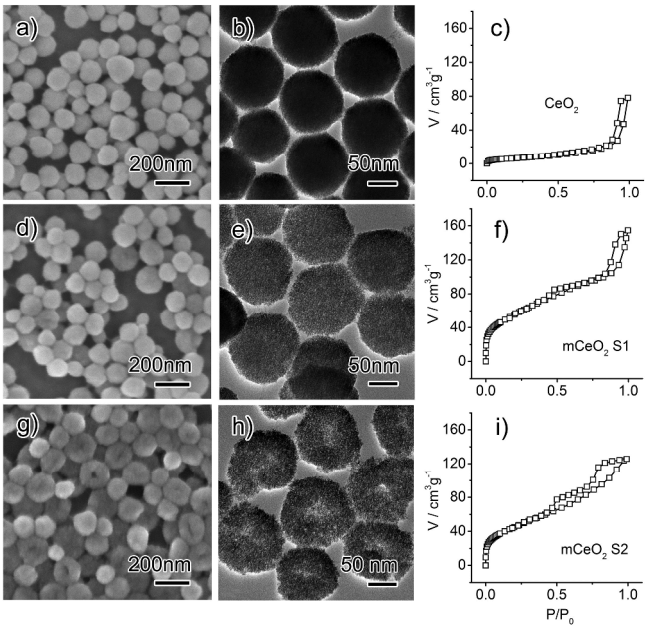

Figure 2. SEM and TEM images of CeO_2 particles during protective etching and N_2 adsorption/desorption isotherms of corresponding products.

The protective etching is constructed based on the interaction and reaction among the substrate particles, the protective agent and the etchant. Therefore, the key to the success of protective etching is the proper selection of involved materials and chemicals.

Table 1. Weight loss of CeO_2 particles etched by HCl solution during the protective etching process, and BET surface areas and average pore size of the corresponding mesoporous CeO_2

Sample	Etching Time (min)	Weight Loss (wt. %)	Surface Area (m^2/g)	Pore Size (nm)
CeO_2	0	0	23.5	4.7
mCeO_2 S1	20	60.8	202.7	5.1
mCeO_2 S2	60	74.5	164.5	4.8
mCeO_2 S3	120	98.8	39.0	6.5

First of all, protective etching prefers "polycrystalline" precursor because it will promote the formation of micro channels within the particle and thereby enhance the etching throughout the particle. For example, the polycrystalline CeO_2 particles (110 nm) are formed by agglomeration of secondary CeO_2 nanocrystals (3.1 nm) during the polyol reaction. The amorphous part between the adjacent nanocrystals is much easier to be etched compared to the individual CeO_2 nanocrystal, so that micro channels along the boundary of crystal domain will form during the etching. It can be proved by the XRD patterns, since there is little change in crystal domain size during etching. (Figure 3) These channels allow the diffusion of etchant into the interior part of the colloid, and facilitate the etching in return, leading to the formation of porous and hollow structures.

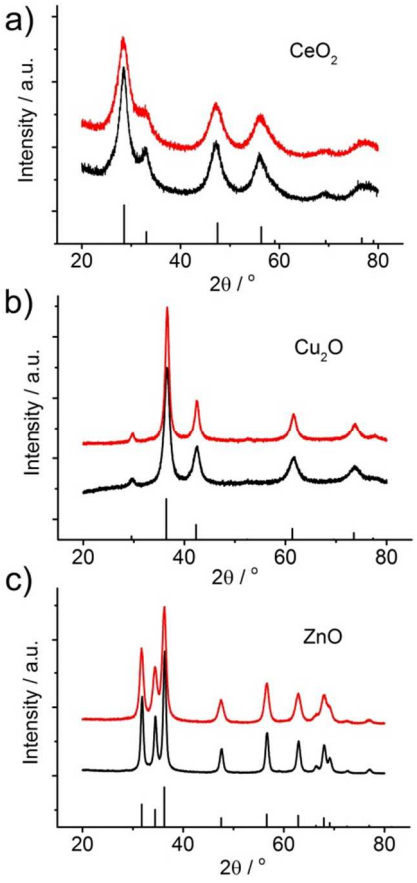

Figure 3. XRD patterns of a) CeO_2 (JCPDF #34-0394), b) Cu_2O (JCPDF #05-0667) and c) ZnO (JCPDF #36-1451) particles before (black) and after (red) acidic etching.

Second, protective etching requires a protective agent with proper combination to the substrate. This interaction should be strong enough to prevent the surface etching but not too strong to completely block the inner etching. Here, PVP is a qualified protective agent with proper combination strength to many metal oxides particles through the coordination between the metal atoms and pyrrole nitrogen or by electrostatic attraction between the surfactant and the particles. The attachment of PVP molecules to the CeO_2 particles can be proved by the FT-IR spectra. (Figure 4) As control samples, surface-clean CeO_2 prepared by high temperature calcination shows the only Ce-O vibration at 400-500 cm^{-1}, while pure PVP shows typical C-N, C=O and C-H vibration around 1560, 1660 and 2800-2900 cm^{-1} respectively. Figure 4 indicates that PVP molecules firmly combine to the CeO_2 particles throughout the whole etching process and PVP molecules can be detected in the precursor particles as well as the mesoporous products.[39, 44] Serving as a protecting agent, the PVP molecules not only increase the stability of surface metal oxides against etching but also prevent the collapse of particles' shell through the connection of neighbouring nanocrystals. Such protection on the surface leads to a relatively higher etching speed inside the substrate particle, which generate mesoporous and hollow nanostructure in sequence. If CeO_2 is synthesized using the same recipe as previous except for a 1/10 amount of PVP, small particles with average diameter of 50 nm can be obtained. These CeO_2 nanoparticles will be completely etched within 10 min due to weak protection from PVP, and no porous products are prepared. (Figure 5) It proved that good PVP protection is essential to the formation of mesoporous structures.

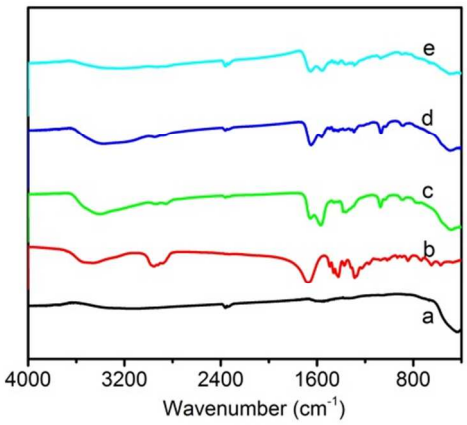

Figure 4. FT-IR spectra of a) CeO_2 after calcination at 700°C, b) PVP, c) as-prepared polyol CeO_2 particles, d) mCeO_2 S1 and e) mCeO_2 S2 particles.

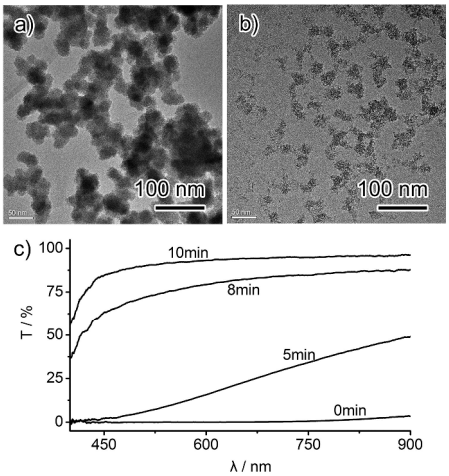

Figure 5. TEM images of less PVP protected CeO_2 particles a) before and b) after 8 min of acid etching, and c) evolution of transmittance of colloidal solution during etching.

Third, protective etching will expect a safe and green etchant with matched etching capabilities related to the specific protective agent. With the help of high reaction temperature, the concentration of acid etchant can be decreased to 0.005-0.3 mol/L according to the specific metal oxide precursor, which decreases the environmental contamination and lower the production cost.

According to the aforementioned mechanism, the broadly used polyol synthesis can be developed to a one-pot reaction for the general preparation of various mesoporous metal oxides. Since most of the polyol synthesized particles are composed of secondary nanocrystals and coated with polymeric surfactant, they are ideal precursors for protective etching. Without additional treatment, the etching process can combine with the polyol reaction seamlessly, which provide a much simplified route to well crystalline mesoporous structures. Actually, we have tried the etching upon the CeO_2, Cu_2O, ZnO precursors, and similar mesoporous structures were produced. (Figure 2, 6, 7) TEM images of all etched particles show a relatively pale contrast and appearance of small holes inside the particles. According to N_2 adsorption/desorption results, the multipoint BET surface area of CeO_2, Cu_2O and ZnO particles increase 8.6 (23.5 – 202.7 m^2/g), 3.8 (10.5 – 40.3 m^2/g) and 3.1 (52.9 – 161.8 m^2/g) times after the etching process. (Table 1-4) XRD patterns indicate the crystal phase and crystal domain size remains unchanged after etching. All these results proved the porous structures are produced by a typical protective etching process. Compared to the alkaline etching to mesoporous silica,[45, 46] the acidic protective etching to metal oxides is scarcely demonstrated. These works together demonstrate that protective etching could be a convenient method and useful supplement to the preparation of mesoporous materials.

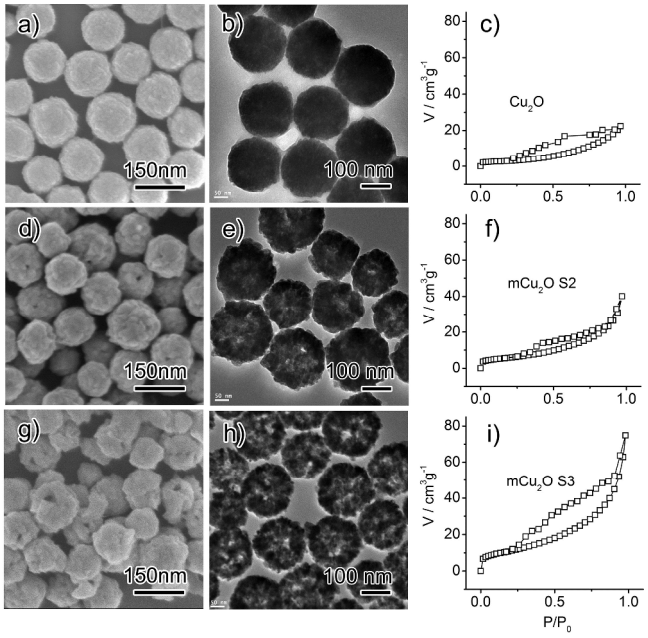

Figure 6. SEM and TEM images of Cu_2O particles during protective etching and N_2 adsorption/desorption isotherms of corresponding products.

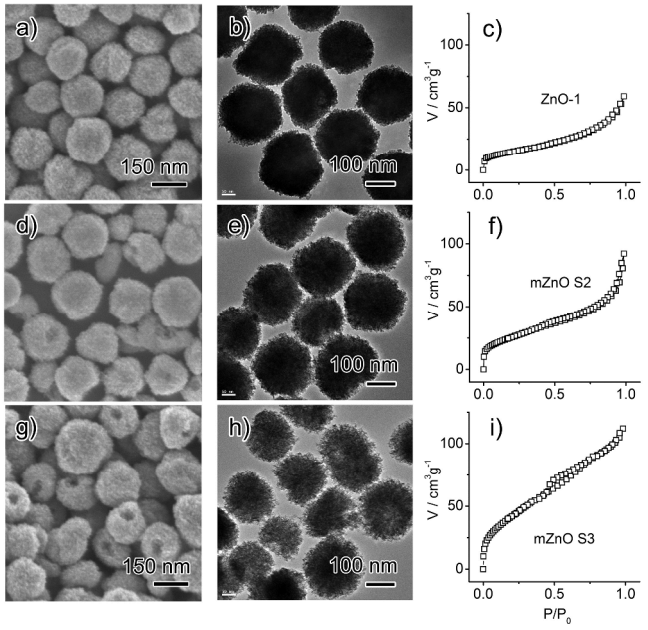

Figure 7. SEM and TEM images of ZnO particles during protective etching and N_2 adsorption/desorption isotherms of corresponding products.

Table 2. Weight loss of Cu_2O particles etched by H_2SO_4 solution with different concentrations for the same 30 minutes, and BET surface areas and average pore size of the corresponding mesoporous Cu_2O.

Sample	9.2M H_2SO_4 (mL)	Weight Loss (wt. %)	Surface Area (m^2/g)	Pore Size (nm)

Cu_2O	0	0	10.5	5.8
mCu_2O S1	0.025	20.6	12.9	8.0
mCu_2O S2	0.075	50	21.0	7.5
mCu_2O S3	0.125	77	40.3	7.2

Table 3. Weight loss of ZnO-1 particles etched by HCl solution with different concentrations for the same 20 minutes, and corresponding BET surface areas and average pore size.

Sample	37% HCl (mL)	Weight Loss (wt. %)	Surface Area (m^2/g)	Pore Size (nm)
ZnO-1	0	0	52.9	6.9
mZnO S1	0.05	12	78.3	6.6
mZnO S2	0.1	44	93.1	6.7
mZnO S3	0.15	65	161.8	4.3

Table 4. Weight loss of ZnO-2 particles etched by HCl solution with different concentrations for the same 5 minutes, and corresponding BET surface areas and average pore size.

Sample	37% HCl (mL)	Weight Loss (wt. %)	Surface Area (m^2/g)	Pore Size (nm)
ZnO-2	0	0	62.8	6.0
mZnO S4	0.35	64.8	91.1	5.7
mZnO S5	0.375	78.6	88.7	6.7

In protective etching, the products' porosity can be controlled by the etching time, the etchant concentration and the crystal domain size of the substrate particles. Here, the adjustment through etching time will be discussed in detail. As shown in Figure 2 and Table 1, the original CeO_2 particle has a deep contrast in TEM image, and its low surface area (23 m^2/g) is consistent with typical values of most nonporous particles. After 20 min of etching, the yellow slurry suspension changes to a more transparent orange dispersion, accompanied by a 60.8 wt. % loss for CeO_2. TEM image shows no shrinkage in particle size but a much pale contrast with tiny pores throughout the particles. The surface area increases sharply to 202 m^2/g, which indicating the formation of disordered mesoporous structures. As the etching proceeds to 60 min, reaction solution becomes more transparent with 74.5 wt. % loss of CeO_2. The mesoporous particles gradually change to hollow particle with thick porous shells, and the surface area drops to 164m^2/g due to the hollow structures. Over etching (120 min) causes the collapse of mesoporous particles and almost all CeO_2 dissolve into the solution in the form of Ce^{4+} ions. The analysis of weight loss and related surface area shows that the etching is fast in the first 20 min due to easy removal of poor crystalline CeO_2 content. Then, the etching becomes 10 times slower in the following 40 min as the left well crystalline CeO_2 secondary nanocrystals are more difficult to be etched. In the final stage, these secondary nanocrystals will be eventually etched under long time exposure to the acidic environment. The kinetic study suggests that mesoporous CeO_2 particles can be prepared in the beginning or intermediate stage of etching, while over etching only lead to small amount of fragments.

In addition, the porosity can be controlled by the acid concentration either, where high concentration usually leads to a more porous product within the same etching time. (Figure 6-7, Table 2-4) Furthermore, the crystal domain size of the substrate particles also has significant influence upon the porosity. (Figure 8) With comparable etching degree (65% weight loss), ZnO-1 particles with small grain size (6.7 nm) produce mesoporous ZnO with high surface area (161.8 m^2/g), while ZnO-2 particles with large grain size (13.4 nm) generate mesoporous products with relatively low surface area (91.1 m^2/g). Based on the parallel etching for two ZnO precursors, it can be concluded that the substrate particles with small grain size favors the formation of mesoporous particles with larger surface areas.

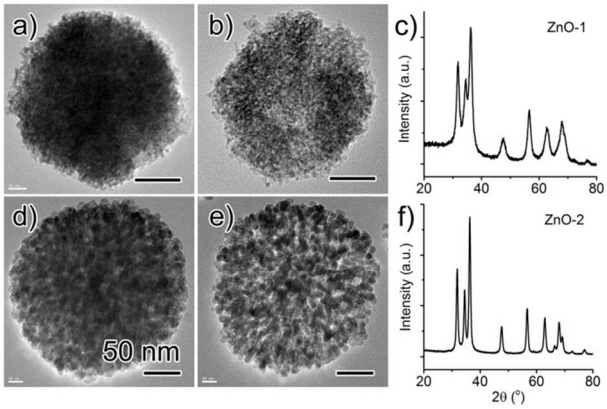

Figure 8. Influence of crystal grain size upon the porosity and surface area of the mesoporous ZnO from protective etching.

The mesoporous metal oxides synthesized by protective etching have great potential in catalysts or supporting materials due to their high surface area, good crystallinity and thermal stability, and convenience in catalyst loading. First of all, the porous structure and large surface area are intrinsically favorable to the heterogeneous catalysis in the aspect of catalyst dispersion and reactant access, as most catalytic reaction takes place at the surface of catalyst or interface between the catalyst and support. Second, the as-prepared metal oxides are well crystallized since the poor crystalline contents have been removed by the etching. The good crystallinity renders the catalyst/support more active surface and high thermal stability in specific reactions. Third, the as-made metal oxides have great convenience in the loading of catalyst via wet chemistry method, because the disordered pores are created by the diffusion of etchant in solution and the liquid catalyst precursor such as the solution of H_2PtCl_6 or $HAuCl_4$ are easy to be distributed uniformly inside the porous matrix.

As a demonstration, the preferential oxidation (PROX) of carbon monoxide was selected as probe reaction to prove the advantages of $mCeO_2$ as catalyst support compared to the general CeO_2 particles. The Pt loading is fixed at 3% by impregnation and deposition, which is confirmed by ICP-AES measurement to insure the same amount of Pt catalyst on each sample. SEM and EDS analysis of Pt-$mCeO_2$ prove that each particle is composed of Pt, Ce and O elements, and the atom ratio is consistent with the chemical composition. A uniformly dark contrast of Pt-$mCeO_2$ in TEM image compared to that of $mCeO_2$ also proves the existence and good dispersion of Pt nanocrystals throughout the particles. (Figure 9) Furthermore, dark field TEM image of Pt-$mCeO_2$ particles and the elementary mapping also proved the uniform distribution of Pt throughout the $mCeO_2$ particles. (Figure 10) The details of the reaction parameters such as the flow rate of reactants and carrier gas are summarized in Table 5. For the oxidation of CO in absence of H_2 (Figure 11a), both catalysts initiate the conversion at 30 °C, and their activity increases as the temperature rise to 100 °C. Compared to the Pt-CeO_2 catalyst, the Pt-$mCeO_2$ catalyst triggers a relatively higher conversion of CO at

each temperature within this range, and possesses a 10 °C lower light off temperature when 50% of conversion is reached. For the preferential oxidation of CO with presence of excessive H_2 (Figure 11b), whose concentration is 50 times as that of O_2 or CO, the selectivity of both catalysts decrease as the temperature increases due to the increase of formate species,[47] but the selectivity for Pt-mCeO_2 catalyst is always higher than that of Pt-CeO_2 catalyst. It is broadly accepted that CO molecules are majorly adsorbed on the surface of Pt and its oxidation take place at the interface of Pt and CeO_2, while H_2 oxidizes on either CeO_2 or platinum oxide. [43, 47] Therefore, the mesoporous ceria with higher surface area will result in better dispersion of Pt catalyst and larger metal/oxide interface, which lead to higher catalytic activity and better selectivity in CO oxidation.

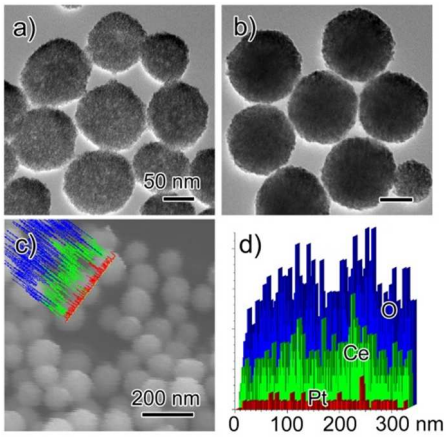

Figure 9. TEM images of a) mCeO_2 and b) Pt-mCeO_2 particles through impregnation method, and c, d) EDS analysis of Pt-mCeO_2 particles as nanocatalysts.

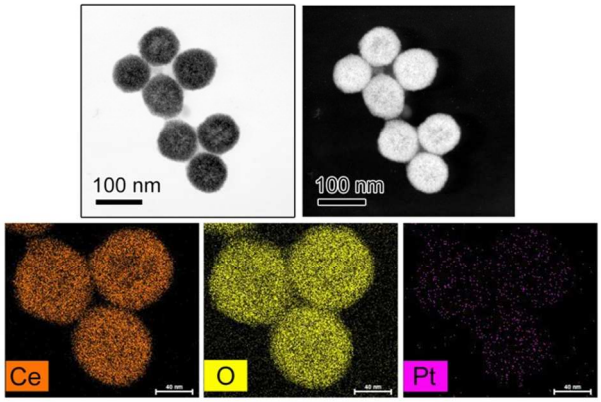

Figure 10. Bright field and dark field TEM image of Pt-mCeO_2 particles, and the mapping of elementary distribution performed by TEM.

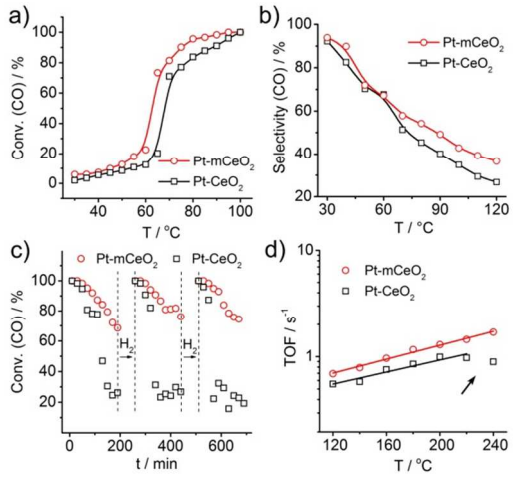

Figure 11. Influence of temperature upon a) conversion and b) selectivity of CO oxidation catalyzed by 3 % Pt-mCeO_2 and Pt-CeO_2 composite particles. c) Comparison of life time of these two catalysts in recycling reactions. d) Turn-over frequency of CO oxidation catalyzed by the two catalysts.

Table 5. Reaction conditions for the catalytic oxidation of CO, including flow rate of CO, O_2 and H_2, reaction temperature and catalyst compositions. No. 1-2, 3-4, 5-6, 7-8 illustrate the catalysis in Figure 9a, 9b, 9c and 9d, respectively.

	4% CO/N_2 (mL/min)	4% O_2/N_2 (mL/min)	H_2 (mL/min)	Reaction Temp. (°C)	Catalyst
1	25	25	/	30-110	3% Pt-CeO_2 (50 mg)
2	25	25	/	30-110	3% Pt-mCeO_2 (50 mg)
3	12.5	12.5	25	30-110	3% Pt-CeO_2 (50 mg)
4	12.5	12.5	25	30-110	3% Pt-mCeO_2 (50 mg)
5	25	25	/	90	3% Pt-CeO_2 (50 mg)
6	25	25	/	90	3% Pt-mCeO_2 (50 mg)
7	100	100	/	120-240	3% Pt-CeO_2 (3.2 mg) + quartz sand (28mg)
8	100	100	/	120-240	3% Pt-mCeO_2 (2.8 mg) + quartz sand (28.4 mg)

In addition to activity and selectivity, the Pt-mCeO_2 catalyst also has better performance in the test of life time and thermo stability. Both the Pt-CeO_2 and the Pt-mCeO_2 catalysts are first tested in 3 continuous oxidation of CO at 90 °C to evaluate their life time. (Figure 11c) After 3hour reaction in each cycle, the catalyst was regenerated by heating under H_2 flow for 70 min to reduce the oxide content on the surface Pt nanocrystals. In the first cycle, Pt-mCeO_2 catalyst can maintain 90% conversion of CO for 90 minutes and the conversion after 3-hour reaction decreases to 70%. While the Pt-CeO_2 catalyst can maintain 90% of conversion for only 50 minutes,

and the final conversion decreases to about 25%. In the following two cycles, the Pt-mCeO_2 catalyst shows the same decay of conversion, but the Pt-CeO_2 catalyst lose its activity faster and faster. Apparently, Pt-mCeO_2 catalyst has not only better activity but also much longer life time in single reaction, probably because the mCeO_2 possesses larger surface area for the competitive absorption and storage of oxygen, which decreases the oxidation on Pt surface and slows the deactivation rate. Therefore, the Pt-mCeO_2 catalyst can be repeatedly used in cycling reaction with help of proper regeneration.

Furthermore, the mesoporous CeO_2 support also relieve the sintering of Pt nanocrystals, which renders the catalyst good thermo stability even at high reaction temperature. (Figure 11d) The turn over frequency of mCeO_2-Pt catalyst monotonically increased with the temperature, while it shows a deviation from linear curve at high temperature for Pt catalyst loaded on unetched CeO_2, which may be attributed to the agglomeration of Pt nanocrystals on the particle surface. All the above comparisons suggests that the as-prepared mesoporous CeO_2 support favors the good dispersion of Pt nanocrystal and function of synergetic interaction between catalyst and support, which create more active sites in catalysis.

4. Conclusions

In summary, a protective etching method is developed to prepare mesoporous CeO_2, Cu_2O and ZnO nanoparticles in one-pot reaction. Polycrystalline precursor particles, protective agent with proper combination to the precursor and etchant with matched etching capability are three preconditions to construct the protective etching system. Due to the polycrystalline characteristics and universal PVP attachment for polyol synthesized particles, the traditional polyol process can be extended to a one-pot reaction for the preparation of mesoporous metal oxides, simply by addition of low concentration inorganic acid into the solution. The products' porosity and surface area can be controlled by the etching time, the etchant concentration and the crystal domain size of the substrate particles. Compared to the widely used nanocasting method to prepare mesoporous metal oxides, which involves the preparation of mesoporous template, the introduction and synthesis of metal oxides and the removal of template, the current etching method provides an alternative and simplified way to produce mesoporous materials with large surface area and good crystallinity. Loading Pt nanocrystal on mCeO_2 rather than unetched CeO_2 particles generate a superior nanocatalyst, which possess better activity, higher selectivity, longer catalytic duration and good thermo stability in CO oxidation reaction. It is believed that the protective etching process will become a useful method for the preparation of porous structures, and its potential in large scale production will provide abundant materials for catalytic applications.

Acknowledgements

J. Ge thanks National Science Foundation of China (21222107, 21471058), Shanghai Rising-Star Program (13QA1401400) and Youth Talent Plan (Organization Department of the Central Committee of the CPC) for support.

Notes and references

[a] Department of Chemistry, Tongji University, Shanghai, China, 200092.
[b] Department of Chemistry, Shanghai Key Laboratory of Green Chemistry and Chemical Processes, East China Normal University, Shanghai, China, 200062.

1. Y. Shi, Y. Wan and D. Zhao, *Chem. Soc. Rev.*, 2011, **40**, 3854-3878.
2. D. Gu and F. Schueth, *Chem. Soc. Rev.*, 2014, **43**, 313-344.
3. Y. Ren, Z. Ma and P. G. Bruce, *Chem. Soc. Rev.*, 2012, **41**, 4909-4927.
4. H. Yen, Y. Seo, S. Kaliaguine and F. Kleitz, *Angew. Chem. Int. Ed.*, 2012, **51**, 12032-12035.
5. J. Kang, Y. Rao, M. Trudeau and D. Antonelli, *Angew. Chem. Int. Ed.*, 2008, **47**, 4896-4899.
6. K. An, S. Alayoglu, N. Musselwhite, S. Plamthottam, G. Melaet, A. E. Lindeman and G. A. Somorjai, *J. Am. Chem. Soc.*, 2013, **135**, 16689-16696.
7. M.-b. Zheng, J. Cao, S.-t. Liao, J.-s. Liu, H.-q. Chen, Y. Zhao, W.-j. Dai, G.-b. Ji, J.-m. Cao and J. Tao, *J. Phys. Chem. C*, 2009, **113**, 3887-3894.
8. A. Walcarius, *Chem. Soc. Rev.*, 2013, **42**, 4098-4140.
9. M. C. Orilall and U. Wiesner, *Chem. Soc. Rev.*, 2011, **40**, 520-535.
10. H. Liu, G. Wang, J. Liu, S. Qiao and H. Ahn, *J. Mater. Chem.*, 2011, **21**, 3046-3052.
11. H. Liu, Z. Bi, X.-G. Sun, R. R. Unocic, M. P. Paranthaman, S. Dai and G. M. Brown, *Adv. Mater.*, 2011, **23**, 3450-3454.
12. T. Brezesinski, J. Wang, J. Polleux, B. Dunn and S. H. Tolbert, *J. Am. Chem. Soc.*, 2009, **131**, 1802-1809.
13. T. Waitz, T. Wagner, T. Sauerwald, C.-D. Kohl and M. Tiemann, *Adv. Funct. Mater.*, 2009, **19**, 653-661.
14. T. Wagner, S. Haffer, C. Weinberger, D. Klaus and M. Tiemann, *Chem. Soc. Rev.*, 2013, **42**, 4036-4053.
15. B. Z. Tian, X. Y. Liu, H. F. Yang, S. H. Xie, C. Z. Yu, B. Tu and D. Y. Zhao, *Adv. Mater.*, 2003, **15**, 1370-1374.
16. S. Lepoutre, B. Julian-Lopez, C. Sanchez, H. Amenitsch, M. Linden and D. Grosso, *J. Mater. Chem.*, 2010, **20**, 537-542.
17. J. Deng, L. Zhang, H. Dai, Y. Xia, H. Jiang, H. Zhang and H. He, *J. Phys. Chem. C*, 2010, **114**, 2694-2700.
18. P. D. Yang, D. Y. Zhao, D. I. Margolese, B. F. Chmelka and G. D. Stucky, *Chem. Mater.*, 1999, **11**, 2813-2826.
19. B. Lee, D. L. Lu, J. N. Kondo and K. Domen, *J. Am. Chem. Soc.*, 2002, **124**, 11256-11257.
20. F. Jiao and P. G. Bruce, *Angew. Chem. Int. Ed.*, 2004, **43**, 5958-5961.
21. D. Chandra, S. Mridha, D. Basak and A. Bhaumik, *Chem. Commun.*, 2009, 2384-2386.
22. Y. Deng, J. Wei, Z. Sun and D. Zhao, *Chem. Soc. Rev.*, 2013, **42**, 4054-4070.
23. C. Yu, L. Zhang, J. Shi, J. Zhao, J. Gao and D. Yan, *Adv. Funct. Mater.*, 2008, **18**, 1544-1554.
24. L. Tian, H. Zou, J. Fu, X. Yang, Y. Wang, H. Guo, X. Fu, C. Liang, M. Wu, P. K. Shen and Q. Gao, *Adv. Funct. Mater.*, 2010, **20**, 617-623.
25. S. Xiong, J. S. Chen, X. W. Lou and H. C. Zeng, *Adv. Funct. Mater.*, 2012, **22**, 861-871.
26. T. K. Kim, K. J. Lee, J. Y. Cheon, J. H. Lee, S. H. Joo and H. R. Moon, *J. Am. Chem. Soc.*, 2013, **135**, 8940-8946.
27. J.-K. Sun and Q. Xu, *Energy & Environmental Science*, 2014, **7**, 2071-2100.
28. J. H. Lee, Y. J. Sa, T. K. Kim, H. R. Moon and S. H. Joo, *Journal of Materials Chemistry A*, 2014, **2**, 10435-10443.
29. X. Xu, R. Cao, S. Jeong and J. Cho, *Nano Lett.*, 2012, **12**, 4988-4991.
30. X. Liang, J. Xiao, B. Chen and Y. Li, *Inorg. Chem.*, 2010, **49**, 8188-8190.
31. Z. Yang, J. Wei, H. Yang, L. Liu, H. Liang and Y. Yang, *Eur. J. Inorg. Chem.*, 2010, 3354-3359.

32. J. Yu and J. Zhang, *Dalton Trans.*, 2010, **39**, 5860-5867.
33. F. Liu, S. Zuo, X. Xia, J. Sun, Y. Zou, L. Wang, C. Li and C. Qi, *Journal of Materials Chemistry A*, 2013, **1**, 4089-4096.
34. B. Feng, W. Dingsheng, H. Ziyang, C. Wei, L. Liping, L. Xin, C. Chen, W. Xun, P. Qing and L. Yadong, *Angewandte Chemie International Edition*, 2007, **46**, 6650-6653.
35. Q. Zhang, I. Lee, J. Ge, F. Zaera and Y. Yin, *Adv. Funct. Mater.*, 2010, **20**, 2201-2214.
36. Q. Zhang, T. R. Zhang, J. P. Ge and Y. D. Yin, *Nano Lett.*, 2008, **8**, 2867-2871.
37. H. Zeng, W. Cai, P. Liu, X. Xu, H. Zhou, C. Klingshirn and H. Kalt, *ACS Nano*, 2008, **2**, 1661-1670.
38. K. Cheng, S. Peng, C. Xu and S. Sun, *J. Am. Chem. Soc.*, 2009, **131**, 10637-10644.
39. N. Izu, T. Uchida, I. Matsubara, T. Itoh, W. Shin and M. Nishibori, *Mater. Res. Bull.*, 2011, **46**, 1168-1176.
40. J. C. Park, J. Kim, H. Kwon and H. Song, *Adv. Mater.*, 2009, **21**, 803-807.
41. Z. C. Orel, A. Anzlovar, G. Drazic and M. Zigon, *Cryst. Growth Des.*, 2007, **7**, 453-458.
42. D. Jezequel, J. Guenot, N. Jouini and F. Fievet, *J. Mater. Res.*, 1995, **10**, 77-83.
43. A. Wootsch, C. Descorme and D. Duprez, *J. Catal.*, 2004, **225**, 259-266.
44. C. M. Ho, J. C. Yu, T. Kwong, A. C. Mak and S. Y. Lai, *Chem. Mater.*, 2005, **17**, 4514-4522.
45. Q. Zhang, T. Zhang, J. Ge and Y. Yin, *Nano Lett.*, 2008, **8**, 2867-2871.
46. L. You, T. Wang and J. Ge, *Chemistry-a European Journal*, 2013, **19**, 2142-2149.
47. O. Pozdnyakova, D. Teschner, A. Wootsch, J. Krohnert, B. Steinhauer, H. Sauer, L. Toth, F. C. Jentoft, A. Knop-Gericke, Z. Paal and R. Schlogl, *J. Catal.*, 2006, **237**, 1-16.